



Electrodeposited CdZnS/CdS/CIGS/Mo: Characterization and Solar Cell Performance

AMAL BOUICH,^{1,3,4} SHAFI ULLAH,^{1,2} HANIF ULLAH,^{1,2}
MIGUEL MOLLAR,¹ BERNABÉ MARÍ,¹ and MOHAMED EBN TOUHAMI³

1.—Department of Applied Physics, Institute de Disseny i Fabrication, Universitat Politècnica de València, Camí de Vera s/n, 46022 València, Spain. 2.—Electrical Engineering Department, FU-FAST Khayaban-e-Suhrwardy, Islamabad 44000, Pakistan. 3.—Laboratory of Materials Engineering and Environment, University Ibn Tofail BP, 133-14000 Kenitra, Morocco. 4.—e-mail: bouich.amal@gmail.com

Copper indium gallium and di-selenium (CIGS) films have been successfully deposited by the electrodeposition technique. The as-deposited films were annealed at 450°C for 40 min. The (CdS) and cadmium–zinc sulfide (CdZnS) used as buffer and window layer, respectively, were synthesized by the chemical bath deposition technique. The prepared samples were characterized for structure by x-ray diffraction. The morphology of the deposited films was analyzed by scanning electron microscopy. Atomic force microscopy and UV–Vis spectroscopy were used for surface roughness and optical properties. A typical solar cell structure consists of CdZnS–CdS and CIGS–Mo as window, buffer and absorber layer, respectively. The device performance was measured under AM 1.5 global spectrum for 1000 W/m² irradiance, where the obtained efficiencies were in the range of 2–3%. Open-circuit voltage was 345 mV, short circuit current was 16.8 mA/cm² and the fill factor was 38.18%.

INTRODUCTION

Photovoltaic energy is a very precious and effective source that can be used to solve energy problems. Many research projects are aimed at the development and fabrication of solar cell-based on copper indium gallium and di-selenium (CIGS) thin films. CIGS is a semiconductor which can be used for photovoltaic applications due to its electrical and optical properties. CIGS thin films have a higher absorption coefficient ($\sim 1 \times 10^5/\text{cm}$)¹ than silicon-based solar cells,² which have the highest efficiency of 23.8% at the laboratory level.³ Several techniques are available for the fabrication of CIGS thin films. These include laser ablation,⁴ spin coating,⁵ spray pyrolysis,⁶ sputtering,⁷ co-evaporation,⁸ and electrodeposition.⁹ Many attempts have been made to optimize the quality of CIGS films by the addition of complexing agents and buffering agents, and by varying the pH and the temperature of the bath, etc. Electrodeposition is considered to be a low-cost technique with a high deposition rate. It also has the advantage of large area deposition with a high level of thickness control.¹⁰ Nevertheless, efforts are

underway for further improvement of CIGS solar cell efficiency to the theoretical maximum ($\sim 30\%$).¹¹ The fabrication process involves different layers (contact, absorber, buffer, window or reflector, etc.) and the overall performance of the cells depends on the deposition process of the films and their interfaces.

A Mo substrate is usually the back contact in the CIGS configuration. All the CIGS devices use *n*-type cadmium sulfide (CdS) with a thickness of 80–100 nm as a buffer layer which is deposited by using chemical bath deposition (CBD) as in Ref. 12. The CdS film protects the absorber layer against mechanical damage and chemical reactions. This CdS layer also improves and helps the band alignment of the device.¹³ The *p*-type CIGS absorber (1–3 μm thickness) layer is deposited on the Mo-coated glass substrate and the *n*-type front contact transparent bilayer [cadmium–zinc sulfide and zinc oxide (CdZnS, ZnO)] and CdS is deposited on the CIGS thin layer.¹⁴

In this work, we synthesized and characterized thin layers making up CIGS-based solar cells deposited by electrodeposition. To achieve a higher

power conversion efficiency of the device, the window layer (CdZnS, ZnO) and the CdS must transmit a large number of photons to reach the absorber layer and generate electron-hole pairs. The approach is to find alternate materials to replace the toxic CdS buffer layer by using a suitable CBD technique. Furthermore, our device configuration employs a transparent, conductive CdZnS layer with proper doping materials, which makes it easy to minimize the interface alignment and to illuminate the $p-n$ junction. The films were characterized by x-ray diffraction (XRD), scanning electron microscopy (SEM), atomic force microscopy (AFM) and UV-Vis spectroscopy.

EXPERIMENTAL SETUP

CIGS thin layers were electrodeposited by using aqueous solutions of CuCl_2 , InCl_2 , GaCl_2 , and H_2SO_3 . LiCl was used as a supporting electrolyte and the pH of the solution was adjusted to 2.4 by slowly adding concentrated HCl. A three-electrode setup was used with Mo as the back contact, a Pt-plated counter electrode and a Ag/AgCl reference electrode with 0.6 V applied potential.¹⁵ The as-deposited thin films were annealed at 450°C for 40 min to improve the crystallinity.^{16,17}

After annealing the CIGS films, a thin CdS buffer layer was deposited using a simple CBD method. The annealed sample of the CIGS was vertically immersed in a 60-ml-based aqueous solution with pH 11, containing CdSO_4 (0.06 M), thiourea $\text{CH}_4\text{N}_2\text{S}$ (0.75 M) and ammonia for the pH control. The bath temperature was kept at 75°C with continuous magnetic stirring at 600 rpm for 1 h. The yellow thin film was washed with deionized water to remove the loosely bonded particles formed on the surface during deposition, and then the sample was dried.¹⁸

The next step was the n -type window layer deposition, consisting of the above procedure for CdS by adding ZnSO_4 (0.1 M) as a source of Zn^{+2} , and Cd-doped ZnO, forming the CdZnS film. Finally, the finger-patterned film of Au (80 nm) for the electron collection was deposited by using the evaporation method. The device had a SLG/Mo/CIGS/CdS/CdZnS/Au structure.

Structural characterization of the films was carried out by using XRD with Cu-K α radiation ($\lambda = 1.54 \text{ \AA}$). The composition and microstructure of the films were examined using energy dispersive x-ray analysis and SEM. The surface morphology and roughness of the films were analyzed by AFM, and UV-Vis spectroscopy was used for the measurement of the optical properties in the wavelength range of 300–900 nm. The performance of the CIGS-based solar cells were evaluated using a solar simulator under AM 1.5 intensity to obtain the current and voltage ($J-V$) curve characteristics.

RESULTS AND DISCUSSION

XRD analysis of the as-deposited films revealed poor crystallinity. The annealing treatment of the CIGS films at 450°C for 40 min increased the crystallinity of the films, as can be seen from Fig. 1. The appearance of the major peaks matches well with the tetragonal crystal system of the JCPDS No. 075-0104 pattern, corresponding to CuGaSe_2 phase (112), (220/204) and (312). An improvement in crystallinity is indicated following the heat treatment.¹⁹

The thin CdS films annealed at 400°C were analyzed for their structure using XRD. Diffraction peaks corresponded to the (002), (110) and (103) planes with a higher intensity which is an indication of the polycrystallinity of the CdS films.²⁰

On the other hand, the diffraction peaks of the thin-layer CdS doped with 5% of Zn are identified at the same 2θ values, as can be seen in Fig. 2, with a decrease in their intensity. This decrease in intensity is an indication of the decreases in the crystallinity of the ternary CdZnS layer. This result is attributed to the decrease of the lattice parameters of CdZnS that come from substituting Zn^{2+} (88 pm) for Cd^{2+} ions of 109 pm (thus, a smaller atomic size), which leads to a wide-angle influencing the CdS layer's crystallinity.²¹

Figure 3 shows the surface morphology of as-deposited and annealed CIGS samples. The SEM images have a homogenous and smooth surface with a smaller grain size of the as-deposited films. However, granular crystallites were observed in the CIGS thin films, and their size increased with the annealing temperature. This increase in grain size produces a large number of grain boundaries that prevent charge carrier recombination, which causes a significant improvement in the conversion efficiency of the solar cells.²²

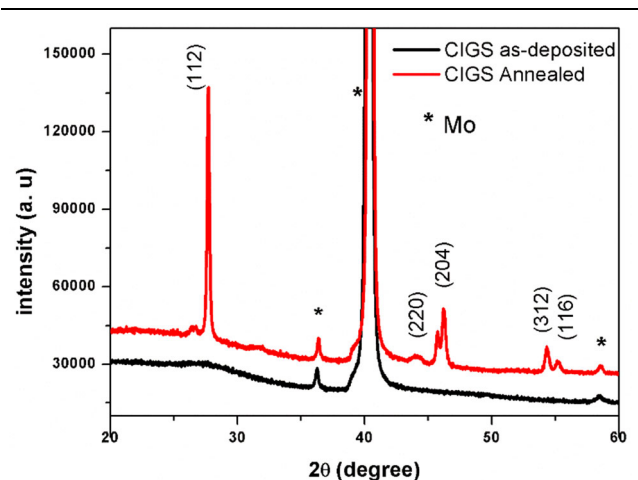


Fig. 1. XRD patterns of electrodeposited CIGS.

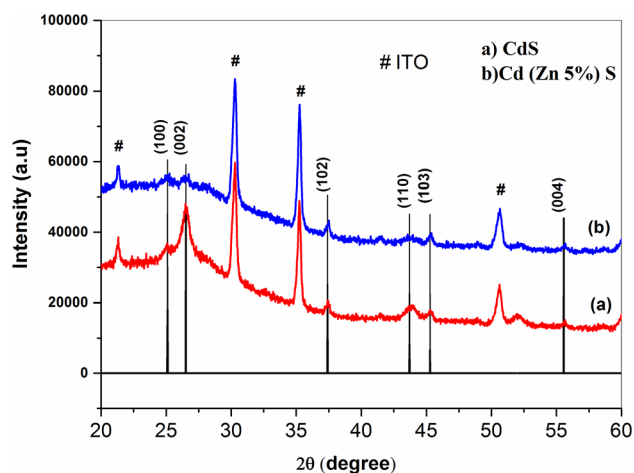


Fig. 2. XRD patterns of deposited (a) CdS and (b) CdZnS layers.

Figure 4 shows the SEM analysis of the CdS and CdZnS thin films. A uniform and smoother fiber-like wire structure was obtained with increases in the Zn content. It can be observed that the decrease in the grain size with Zn content may be useful for solar cell applications using as a window layer.^{23,24}

Figure 5 presents the topography of the CIGS, CdS, and CdZnS thin films analyzed by AFM. It can be seen that the films changed their surfaces to thin and fine particles. According to the AFM analysis this is important for thin films due to its contribution to electrical and mechanical properties, and the surface topography was found to be influenced by the incorporation of the Zn content. The fine roughness and small grains in the films were observed and their size gradually becomes smaller with the Zn content. This is an indication that due to the incorporation of Zn the roughness of the films

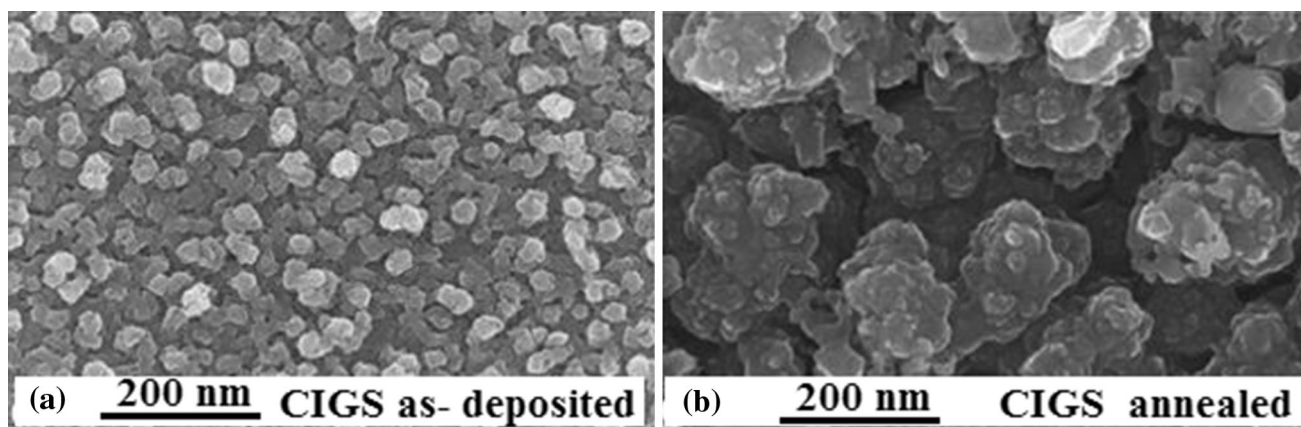


Fig. 3. SEM images of the thin film CIGS: (a) as-deposited and (b) after annealing.

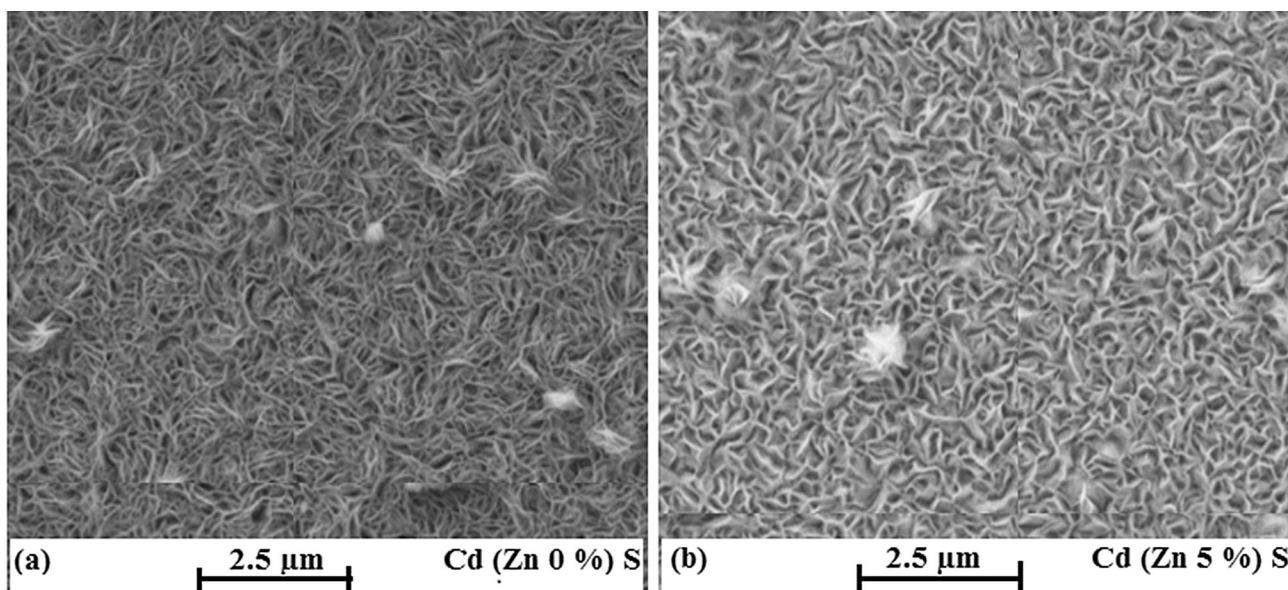


Fig. 4. SEM images of the synthesized films: (a) Cd(Zn 0%)S and (b) Cd(Zn 5%)S.

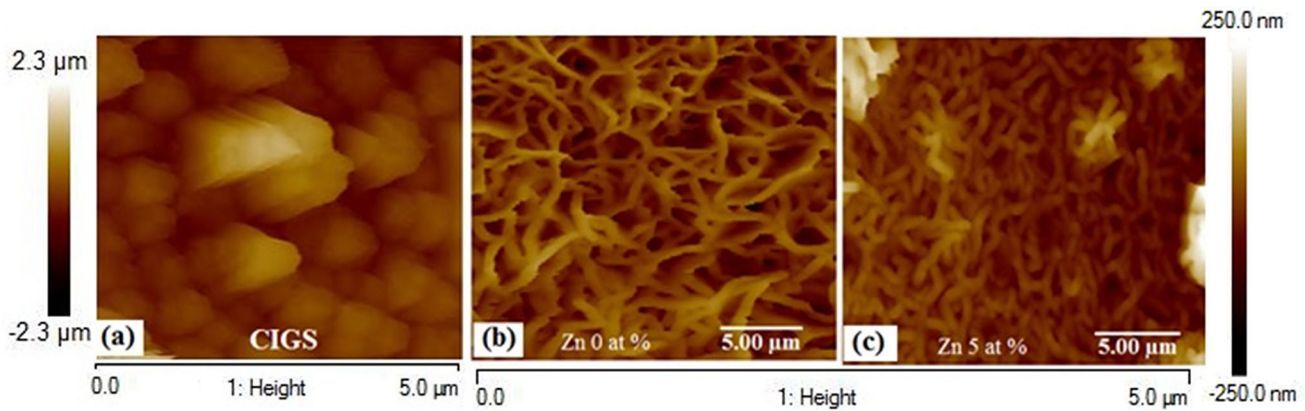


Fig. 5. AFM (2D) images (2D) of surface morphologies: (a) CIGS, (b) CdS, and (c) CdZnS.

decreases. This in turn increases the transmittance of the incident light and prevents recombination to generate more hole–pairs in the absorber layer.

OPTICAL PROPRIETIES

The optical properties of CIGS thin films such as absorbance and bandgap energy varied with wavelength (λ) in the series of 400–900 nm; the material has good absorption in the visible region. The thin CIGS layer is considered a direct bandgap semiconductor material. The bandgap energy was determined from the absorbance data by plotting $(Ah\nu)^2$ versus $h\nu$ to the energy axis at $(Ah\nu)^2 = 0$, where A is the absorbance and $h\nu$ the photon energy.²⁵ The obtained bandgap for CIGS thin films is 1.6 eV which is favorable for the absorber layer, and is shown in Fig. 6.

Figure 7a shows the absorbance of CdS and CdZnS thin films in the wavelength range of 300–650 nm. The optical bandgap was calculated as discussed previously for CdS at 2.48 eV and CdZnS at 3.05 eV (Fig. 7b). The variation in the bandgap energy from 2.48 eV to 3.05 eV is of great interest due to the incorporation of 5 at.% Zn in the CdS, which is considered a promising window layer for CIGS-based solar cells in order to decrease the absorption in the window layer and exhibit a high transmittance over a wide range of wavelength.²⁶

CIGS-BASED SOLAR CELL

The device performance of CIGS-based solar cells configuration shown in Fig. 8a was characterized by measuring the J – V behavior under simulated AM 1.5 illumination (1000 W/m^2). The best device performance is recorded as 2.2% in Fig. 8b. Open-circuit voltage, short circuit current and fill factor ($V_{oc} = 345 \text{ mV}$, $J_{sc} = 16.8 \text{ mA/cm}^2$ and $FF = 38.18\%$) was obtained with a 5% Zn content respectively. The achieved efficiency is relatively lower than those of the literature. We can observe that the device has some natural defects, such as recombination loss at grain boundaries and series resistance, which cannot boost the efficiency of the

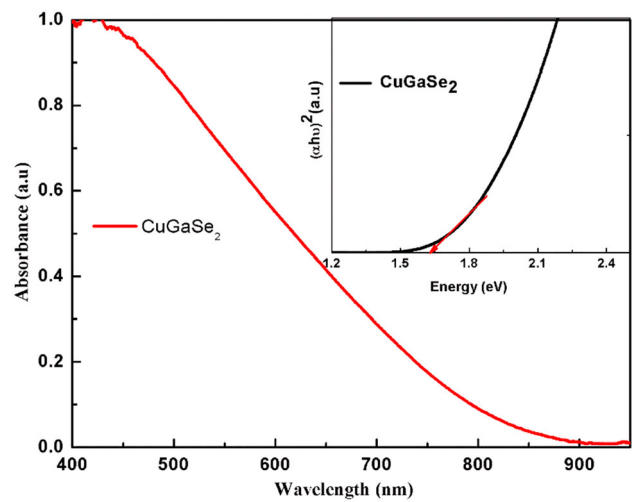


Fig. 6. Optical absorption and bandgap of annealed CIGS.

device. The comparison of our CIGS device with different works fabricated by various techniques is illustrated in Table 1.

CONCLUSION

In this study, a CIGS-based solar cell was proposed, which consisted of a sequential process electrodeposition for a CIGS absorber layer and CBD for the buffer and window layers. The annealing treatment plays an important role in the device performance as it increased the grain size and the crystallinity of the absorber layer to collect more light. The CdS buffer layer and CdS doped with 5 at.% Zn were examined where the following results were observed: (1) a decrease in surface roughness, (2) substitution of Zn for Cd, and (3) an increase in the optical bandgap. The increasing bandgap is an indication for covering the high-energy wavelength in the visible region to transmit high-energy photons. The CIGS-based device fabricated with a 5% Zn content had a conversion efficiency of 2.2%, open-circuit voltage of 345 mV, a short circuit current of 16.8 mA/cm^2 and a fill

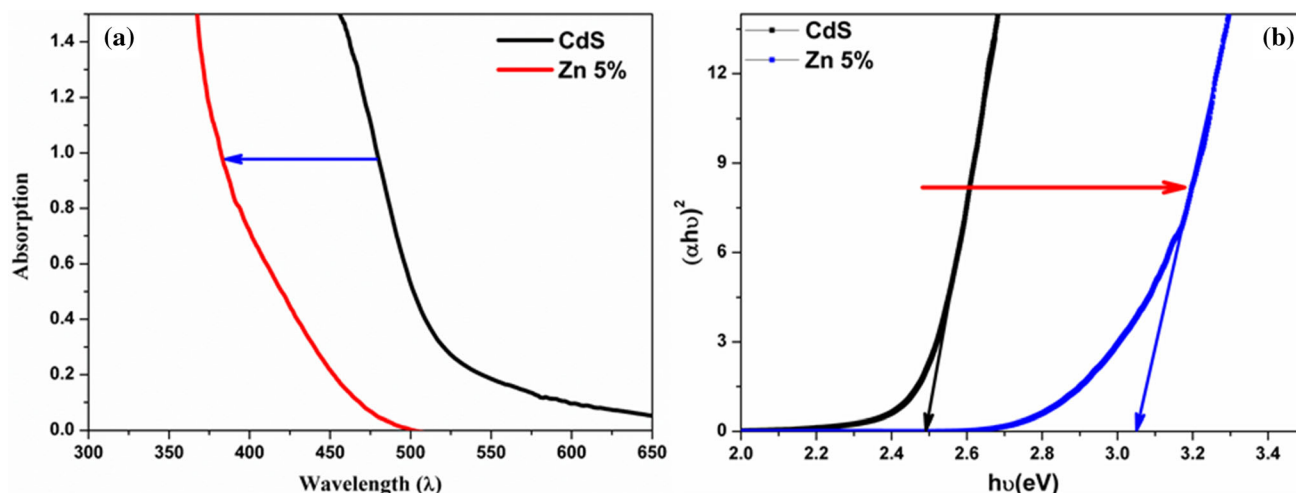


Fig. 7. (a) Optical absorption and (b) bandgap of CdS with Zn content.

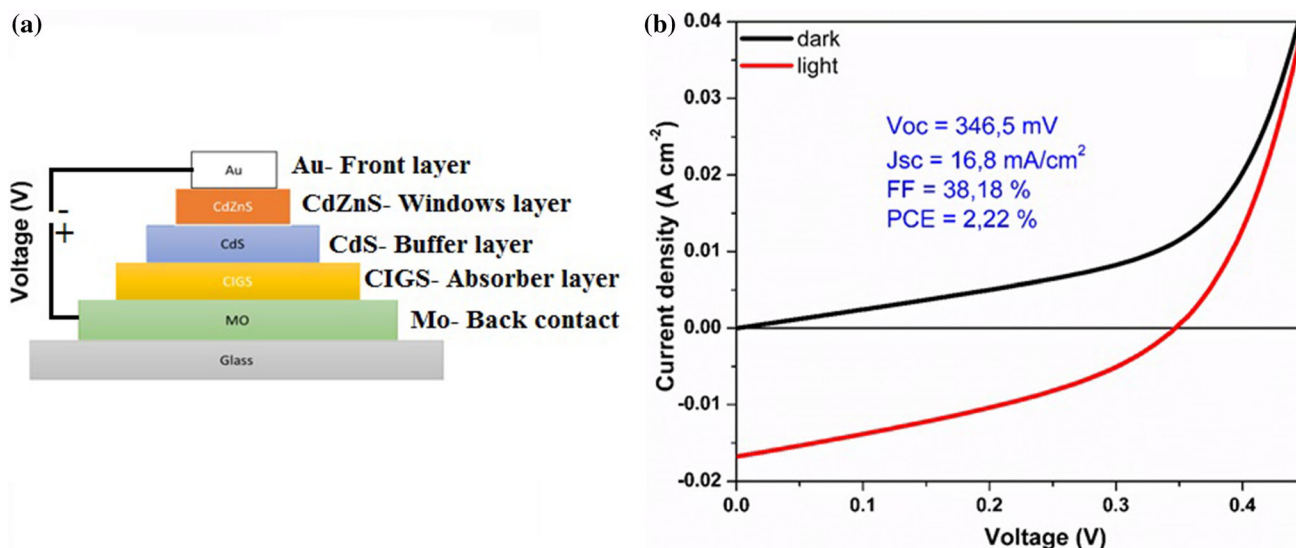


Fig. 8. (a) A typical device SLG/Mo/CIGS/CdS/CdZnS/Au structure configuration, and (b) J - V characteristic curve in the dark and under illumination.

Table 1. Photovoltaic parameters for different CIGS solar cells, including fabrication methods

Cell structure	Fabrication technique	PV parameters				References
		J_{sc} (mA/cm ²)	V_{oc} (mV)	FF (%)	η (%)	
ZnO/CdS/CuGaSe ₂ /Mo	Electrodeposition	14.9	546.0	50.8	4.10	25
ZnO/CdS/CIGS/Mo	Co-evaporation	35.2	538.2	69.6	13.20	26
ZnO/CdS/CIS/ITO	Scalable coating process	25.8	280.0	39.0	2.82	10
ZnO, CdZnS/CdS/CIGS/MO	Electrodeposition and CBD	16.8	346.5	38.18	2.22	Our work

factor of 38.18%. The achieved efficiency is relatively lower than those in the literature, but the proposed study could be an alternative for replacing sputtering-based deposition by CBD to reduce the overall production costs of the device.

ACKNOWLEDGEMENT

We are grateful to the Ministerio de Economía y Competitividad (ENE2016-77798-C4-2-R) for supporting this work.

REFERENCES

1. S.H. Han, A.M. Hermann, F.S. Hasoon, H.A. Al-Thani, and D.H. Levi, *Appl. Phys. Lett.* 85, 576–578 (2004).
2. A. Bouich, B. Hartiti, S. Ullah, H. Ullah, M.E. Touhami, D.M.F. Santos, and B. Mari, *Appl. Phys. A* 125, 579 (2019).
3. S. Marc, T. Matthieu, S. Susanne, and J.D. Phillip, *Phys. Chem. Chem. Phys.* 13, 4292–4302 (2011).
4. C.C. Chen, X. Qi, M.G. Tsai, Y.F. Wu, I.G. Chen, C.Y. Lin, and K.P. Chang, *Surf. Coat. Technol.* 231, 209–213 (2013).
5. S.H. Mousavi, T.S. Müller, and P.W. Oliveira, *J. Colloid Interface Sci.* 382, 48–52 (2012).
6. S. Ahn, K.H. Kim, J.H. Yun, and K.H. Yoon, *J. Appl. Phys.* 105, 113533 (2009).
7. B. Sang, K. Kushiya, D. Okumura, and O. Yamase, *Solar Energy Mater. Solar Cells* 67, 237–245 (2001).
8. S. Jung, S. Ahn, J.H. Yun, J. Gwak, D. Kim, and K. Yoon, *Curr. Appl. Phys.* 10, 990–996 (2010).
9. V.S. Saji, I.H. Choi, and C.W. Lee, *Sol. Energy* 85, 2666–2678 (2011).
10. Z. Li, L. Fang-fang, L. Feng-yan, H. Qing, L. Bao-zhang, and L. Chang-jian, *Solar Energy Mater. Solar Cells* 99, 356–361 (2012).
11. C.D.R. Ludwig, T. Gruhn, F. Claudia, S. Tanja, W. Johannes, and K. Peter, *Phys. Rev. Lett.* 105, 025702/1-4 (2010).
12. D. Hariskos, M. Powalla, N. Chevaldonnet, D. Lincot, A. Schindler, and B. Dimmler, *Thin Solid Films* 387, 179–181 (2001).
13. H.W. Schock and R. Noufi, *Prog. Photovolt. Res. Appl.* 8, 151–160 (2000).
14. I. Repins, M.A. Contreras, B. Egaas, C. DeHart, J. Scharf, C.L. Perkins, B. To, and R. Noufi, *Prog. Photovolt. Res. Appl.* 16, 235–239 (2008).
15. D. Lincot, J.F. Guillemoles, S. Taunier, D. Guimard, J. Six-Kurdi, A. Chaumont, and N. Bodereau, *Sol. Energy* 77, 725–737 (2004).
16. R. Friedfeld, R.P. Raffaele, and J.G. Mantovani, *Solar Energy Mater. Solar Cells* 58, 375–385 (1999).
17. L. Zhang, F.D. Jiang, and J.Y. Feng, *Solar Energy Mater. Solar Cells* 80, 483–490 (2003).
18. M.A. Contreras, M.J. Romero, B. To, F. Hasoon, R. Noufi, S. Ward, and K. Ramanathan, *Thin Solid Films* 403, 204–211 (2002).
19. T. Wada, N. Kohara, S. Nishiwaki, and T. Negami, *Thin Solid Films* 387, 118–122 (2001).
20. M. Stoev and A. Katerski, *J. Mater. Chem.* 6, 377–380 (1996).
21. D. Patidar, N.S. Saxena, and T.P. Sharma, *J. Mod. Opt.* 55, 79–88 (2008).
22. M. Gloeckler, J.R. Sites, and W.K. Metzger, *J. Appl. Phys.* 98, 113704 (2005).
23. M.B. Ård, K. Granath, and L. Stolt, *Thin Solid Films* 361, 9–16 (2000).
24. V.B. Sanap and B.H. Pawar, *J. Optoelectron. Biomed. Mater.* 3, 39–43 (2011).
25. M.E. Calixto, P.J. Sebastian, R.N. Bhattacharya, and R. Noufi, *Solar Energy Mater. Solar Cells* 59, 75–84 (1999).
26. G. Jia, N. Wang, L. Gong, and X. Fei, *Chalcogenide Lett.* 7, 377–383 (2010).

Publisher's Note Springer Nature remains neutral with regard to jurisdictional claims in published maps and institutional affiliations.